JCSU: SCIENCE AND TECHNOLOGY OF MINING AND METALLURGY. (2019) 25: 1-17
DOI:…….

Springer

ISSN: 2095-2899 (Print) 2227-5223 (Online)

Adomian decomposition method simulation of Von Kármán swirling bioconvection nanofluid flow

Accepted April 4th 2019

MD. Shamshuddin[*1], S.R. Mishra[2], O. Anwar Bég[3], A. Kadir[4]

[*1]Department of Mathematics, Vaagdevi College of Engineering, Warangal, Telangana, India.
[2]Department of Mathematics, Siksha 'O'Anusandhan University, Khandagiri, Bhubaneswar, Odisha, India
[3]Fluid Mechanics, Aeronautical/Mechanical Engineering, University of Salford, M54WT, England, UK.
[4]Corrosion/Structures, Aeronautical/Mechanical Engineering, University of Salford, M54WT, England, UK.

Abstract: The study reveals analytically on the 3-dimensional viscous time-dependent gyrotactic bioconvection in swirling nanofluid flow past from a rotating disk. It is known that the deformation of the disk is along the radial direction. In addition to that Stefan blowing is considered. The Buongiorno nanofluid model is taken care of assuming the fluid to be dilute and we find Brownian motion and thermophoresis have dominant role on nanoscale unit. The primitive mass conservation equation, radial, tangential and axial momentum, heat, nano-particle concentration and micro-organism density function are developed in a cylindrical polar coordinate system with appropriate wall (disk surface) and free stream boundary conditions. This highly nonlinear, strongly coupled system of unsteady partial differential equations is normalized with the classical Von Kármán and other transformations to render the boundary value problem into an ordinary differential system. The emerging 11th order system features an extensive range of dimensionless flow parameters i.e. disk stretching rate, Brownian motion, thermophoresis, bioconvection Lewis number, unsteadiness parameter, ordinary Lewis number, Prandtl number, mass convective Biot number, Péclet number and Stefan blowing parameter. Solutions of the system are obtained with developed semi-analytical technique i.e. Adomian decomposition method. Validation of the said problem is also conducted with earlier literature computed by Runge-Kutta shooting technique.

Key words: Nanofluids; Gyrotactic bioconvection; Rotating disk bioreactors; Von Kármán swirling flow; Stefan blowing; Adomian decomposition method (ADM).

Cite this article as: 1111 [J]. Journal of Central South University, 2018, 25(10): . DOI:

1 Introduction

External heat and/or mass transfer from rotating bodies has received considerable attention in engineering sciences. Such flows feature centrifugal forces which can dramatically modify heat and mass transfer rates at the boundary (solid surface). When strong buoyancy forces are present the regime becomes a natural convection one. In the absence of buoyancy forces, forced convection is present. Heat transfer is generally analyzed based on the Fourier heat conduction equation and mass transfer via the Fickian diffusion equation. Many different investigations of rotating flows have been communicated over a wide spectrum of geometrical configurations including cones, ellipses, spheres, cylinders and disks and at different rates of rotation from very slow to extremely high speed. Ma et al. [1] investigated theoretically and experimentally the species diffusion in a rotating cylinder. Further Mohanty et al. [2] studied on cylinders, Anwar Bég et al. [3] on thermo-magnetic free convection boundary layers from a spinning cone in permeable media, Subhashini et al. [4] on compressible heat and mass transfer from a spinning sphere (using

finite difference methods) and Takhar and Whitelaw [5] on asymptotic convection from a rotating sphere. An important geometry in various biochemical and medical processes is the rotating disk apparatus. This is also deployed in petroleum engineering as a mechanism for evaluating the kinetics of heterogeneous reactions [6]. The swirling flow from rotating disks also arises in rotary atomization, photocatalytic fuel cells (RDPFCs) [7] and gas absorption dynamics [8]. The fluid mechanics of rotating disk flow was first evaluated in a monumental study by Von Kármán [9] who introduced his famous set of transformations rendering the Navier-Stokes equations into ordinary differential form. Many studies were communicated subsequently which are summarized in Greenspan [10]. Analyses of heat and mass transfer in Von Kármán flows have been lucidly reviewed more recently by Sehvchuk [11]. Many interesting studies have been conducted focused on either heat, mass or combined heat and mass transfer for both Newtonian and non-Newtonian fluids with multi-physical and chemical effects present. These studies have been communicated by Gambaryan-Roisman and Stephan [12] (considering wall topography and thermo capillary i.e. surface tension effects), Helcig and Wiesche [13] (experimental work considering both air and water).

Recently, nanotechnology is an advanced area of research in engineering. Therefore, Choi [14] initiated the pioneer work on Nanofluids which contribute a emerging role in fluid dynamics due to significant achievements than that of conventional base fluids such as water, kerosene, air, etc with various nano-particles. The suspensions of these nanoparticles have enhanced properties on thermal conductivity and viscosity. Now a day, nanofluids have vast use in biomedical technology. Moreover, nanofluid research and development have extensive experimental investigations. Further, Buongiorno [15] developed a popular model on nanofluid. This suggests the contribution of dynamic role of thermophoresis and Brownian motion on the enhancement of conductivity. Das et al. [16] proposed advanced diverse applications and simulations of nanofluids. Rotating nanofluid flows have more recently garnered some attention. These combine the theory of rotating fluids with nanofluid properties. Use of similar flows which helps in reduction of maximum coordinates for non-linear coupled PDEs into systems of ODEs and they solved either analytically or numerically. Turkyilmazoglu [17] in his proposed study on nanofluid considering water as a base fluid and along with several nanoparticles such as Cu, Ag, CuO, etc. are imposed and for the solution he used spectral Chebyshev collocation method and concluded that copper nanofluids is best for heat transfer. Influence of solutal concentration on swirling disk flow of magnetite ferrous oxide was studied by Hayat et al. [18] and proposed homotopy series solutions. Raza et al. [19] computed magnetized three-dimensional nanofluid flow in a rotating medium using the Buongiorno model.

Bioconvection refers to continuous formation of suspensions of swimming micro-organisms e.g. algae and bacteria. Steady patterns and also the formation of patterns in gyrotatic bioconvection can be strongly regulated by torques. Very sophisticated hydrodynamic models have been developed for the propulsion of such microorganism. Rotating bioconvection has also received considerable interest in recent years. For example, Chakraborty et al. [20] used bvpc function of Matlab to examine impacts of magnetic field and convective boundary conditions. Rotating bio convection in nanofluids is also a rich and emerging area of nano-bio-fluid dynamics which holds some promise for energy systems and medical applications. By suspend micro-organisms in nanofluids, both thermal enhancement benefits and green engineering benefits may be achieved simultaneously. This has inspired some recent activity in mathematical models of nanofluid bio convection in rotating systems. Xun et al. [21] used the MATLAB bvp4c ordinary differential equation solver to compute the nanofluid bio convection in a rotating channel with temperature-dependent viscosity and thermal variable conductivity. They observed that local Nusselt number and wall motile microorganisms flux are more significantly modified by thermal conductivity variation parameter and that larger values of bio convection Péclet number result in an accumulation of motile microorganisms in the core region of the channel. They further noted that this accumulation is intensified with thermophoresis but inhibited with Brownian motion.

In the above studies whether they involve nanofluids or bio convection or both, the boundary walls have generally been rigid. However

deformable boundaries are increasingly featuring in modern biomedical designs. For example, microbial cell engaged in imposing bio convection in nanofluids are exploring stretching (and contracting) walls which can dramatically influence microorganism impacts heavily on fuel cell efficiency and sustainability. Recently Anwar Bég et al. [22] worked on stretching/shrinking) in a deformable channel as a model for bio convection nanofluid fuel cell. They showed that doping of the base fluid with nanoparticles and suspended gyrotactic microorganisms collectively enhances both nanoparticle and motile microorganism mass wall flux (Sherwood numbers) and generally, a stable mixture (suspension) is attained. Several authors (Li et al. [23], Imtiaz et al. [24], Hayat et al. [25] and Hayat et al. [26]) have proposed their work on bio convection nanofluid transport, in various model considering different nanofluids like magnetite-Fe3O4 ferro-nanofluid, CNT nanofluid etc. Other studies include Ahmed et al. [27] (for magneto-nanofluid squeezed between parallel disk), Mushtaq and Mustafa [28] (for nanofluids with convective mass wall conditions) and Chen et al. [29] (considering power-law stretching of the disk for gyrotactic bio Nano convection flow). From the aforesaid studies it is to note that stretching disk is useful for the distribution of temperature, nanoparticle concentration and motile micro-organism density.

In the current study, we re-visit the recent investigation by Latiff et al. [30] to generalize their analysis of time-dependent Von Kármán swirl bio convection nanofluid flow from a rotating disk with Stefan blowing (wall mass transfer) and radial disk stretching. Thermophile (“heat loving”) gyrotactic micro-organism bio convection is addressed. Stefan blowing is a more sophisticated mechanism for studying wall mass transfer than conventional transpiration (injection velocity) models. The present nonlinear coupled partial differential equation boundary value problem is normalized with appropriate transformations into ordinary differential form. An optimized Adomian decomposition method based on power-series expansions is utilized to solve the dimensionless governing equations. The results of Latiff et al. [30] are verified. Extensive new computations are also presented which provide a wider insight into the mechanisms of transport in the boundary layer swirl regime. The simulations presented are relevant to biofilm rotating disk reactors modified with nano-particle doping. Furthermore, these studies provide a useful benchmark for more complex computational fluid dynamics analysis with commercial codes (e.g. ANSYS FLUENT) which will be of benefit to bio-nano-fuel cell designers.

2 Mathematical vonkármán swirl bioconvection nanofluid model

Considered an unsteady 3D bioconvection nanofluid over a rotating disk in a cylindrical polar coordinate system (r, θ,z) with velocity components (u,v,w). The nanofluid is assumed to be a dilute suspension with a homogenous distribution of gyrotatic micro-organisms. Gyrotaxis is swimming directed by the balance between the torque due to gravity acting on a bottom-heavy cell and the torque due to viscous forces arising from local shear flows. In the present model the micro-organisms do not interact with the nano-particles. Similar to nanofluids, in suspensions of motile microorganisms that exhibit spontaneous formation of flow patterns (this phenomenon is called bioconvection) physical laws that govern smaller scales lead to a phenomenon visible on a larger scale. At the disk surface no-slip boundary conditions are considered with Stefan’s blowing and simulated along axial velocity component. From Figure 1 the species concentration of nanofluid at the disk surface follow $C_f > C_w > C_\infty$ to impose mass convective conditions. Due to various nanoparticle concentration near to the disk concentration, wall and ambient states needs mass transfer coefficient h_m. .From the aforesaid assumptions, the governing equations for continuity, radial, circumferential (azimuthal) and axial momentum, thermal energy (heat), nanoparticle concentration (species volume fraction)and motile microorganism density number, in cylindrical coordinates are as follows [30]:

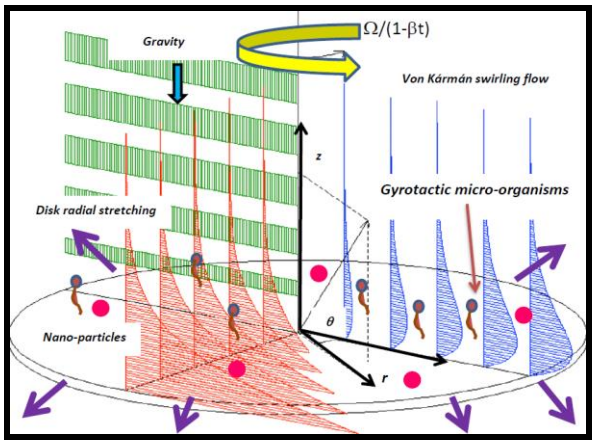

Figure 1 Flow configuration of problem

$$\frac{\partial \bar{u}_{\bar{r}}}{\partial \bar{r}}+\frac{\bar{u}_{\bar{r}}}{\bar{r}}+\frac{\partial \bar{u}_{\bar{z}}}{\partial \bar{z}}=0 \tag{1}$$

$$\frac{\partial \bar{u}_{\bar{r}}}{\partial \bar{t}}+\bar{u}_{\bar{r}}\frac{\partial \bar{u}_{\bar{r}}}{\partial \bar{r}}+\bar{u}_{\bar{z}}\frac{\partial \bar{u}_{\bar{r}}}{\partial \bar{z}}-\frac{\bar{u}_{\theta}^{2}}{\bar{r}}=-\frac{1}{\rho}\frac{\partial \bar{P}}{\partial \bar{r}}+\nu\left(\frac{\partial^{2}\bar{u}_{\bar{r}}}{\partial \bar{r}^{2}}+\frac{\partial^{2}\bar{u}_{\bar{\theta}}}{\partial \bar{z}^{2}}+\frac{1}{\bar{r}}\frac{\partial \bar{u}_{\bar{r}}}{\partial \bar{r}}-\frac{\bar{u}_{\bar{r}}}{\bar{r}^{2}}\right) \tag{2}$$

$$\frac{\partial \bar{u}_{\theta}}{\partial \bar{t}}+\bar{u}_{\bar{r}}\frac{\partial \bar{u}_{\theta}}{\partial \bar{r}}+\bar{w}\frac{\partial \bar{u}_{\theta}}{\partial \bar{z}}-\frac{\bar{u}_{\bar{r}}\bar{u}_{\theta}}{\bar{r}}=\nu\left(\frac{\partial^{2}\bar{u}_{\theta}}{\partial \bar{r}^{2}}+\frac{\partial^{2}\bar{u}_{\theta}}{\partial \bar{z}^{2}}+\frac{1}{\bar{r}}\frac{\partial \bar{u}_{\theta}}{\partial \bar{r}}-\frac{\bar{u}_{\theta}}{\bar{r}^{2}}\right) \tag{3}$$

$$\frac{\partial \bar{u}_{\bar{z}}}{\partial \bar{t}}+\bar{u}_{\bar{r}}\frac{\partial \bar{u}_{\bar{z}}}{\partial \bar{r}}+\bar{u}_{\bar{z}}\frac{\partial \bar{u}_{\bar{z}}}{\partial \bar{z}}=-\frac{1}{\rho}\frac{\partial \bar{P}}{\partial \bar{z}}+\nu\left(\frac{\partial^{2}\bar{u}_{\bar{z}}}{\partial \bar{r}^{2}}+\frac{\partial^{2}\bar{u}_{\bar{z}}}{\partial \bar{z}^{2}}+\frac{1}{\bar{r}}\frac{\partial \bar{u}_{\bar{z}}}{\partial \bar{r}}\right) \tag{4}$$

$$\frac{\partial \bar{T}}{\partial \bar{t}}+\bar{u}_{\bar{r}}\frac{\partial \bar{T}}{\partial \bar{r}}+\bar{u}_{\bar{z}}\frac{\partial \bar{T}}{\partial \bar{z}}=\alpha\left(\frac{\partial^{2}\bar{T}}{\partial \bar{r}^{2}}+\frac{1}{\bar{r}}\frac{\partial \bar{T}}{\partial \bar{r}}+\frac{\partial^{2}\bar{T}}{\partial \bar{z}^{2}}\right)+\tau\left(D_{B}\left(\frac{\partial \bar{T}}{\partial \bar{r}}\frac{\partial \bar{C}}{\partial \bar{r}}+\frac{\partial \bar{T}}{\partial \bar{z}}\frac{\partial \bar{C}}{\partial \bar{z}}\right)+\frac{D_{T}}{T_{M}}\left[\left(\frac{\partial \bar{T}}{\partial \bar{y}}\right)^{2}+\left(\frac{\partial \bar{T}}{\partial \bar{z}}\right)^{2}\right]\right) \tag{5}$$

$$\frac{\partial \bar{C}}{\partial \bar{t}}+\bar{u}_{\bar{r}}\frac{\partial \bar{C}}{\partial \bar{r}}+\bar{u}_{\bar{z}}\frac{\partial \bar{C}}{\partial \bar{z}}=D_{B}\left(\frac{\partial^{2}\bar{C}}{\partial \bar{r}^{2}}+\frac{1}{\bar{r}}\frac{\partial \bar{C}}{\partial \bar{r}}+\frac{\partial^{2}\bar{C}}{\partial \bar{z}^{2}}\right)+\frac{D_{T}}{T_{M}}\left(\frac{\partial^{2}\bar{T}}{\partial \bar{r}^{2}}+\frac{1}{\bar{r}}\frac{\partial \bar{T}}{\partial \bar{r}}+\frac{\partial^{2}\bar{T}}{\partial \bar{z}^{2}}\right) \tag{6}$$

$$\frac{\partial \bar{n}}{\partial \bar{t}}+\bar{u}_{\bar{r}}\frac{\partial \bar{n}}{\partial \bar{r}}+\bar{u}_{\bar{z}}\frac{\partial \bar{n}}{\partial \bar{z}}+\frac{\tilde{b}W_{c}}{\bar{C}_{\infty}}\left[\frac{\partial}{\partial \bar{z}}\left(\bar{n}\frac{\partial \bar{C}}{\partial \bar{z}}\right)\right]=D_{n}\left(\frac{\partial^{2}\bar{n}}{\partial \bar{r}^{2}}+\frac{\partial^{2}\bar{n}}{\partial \bar{z}^{2}}+\frac{1}{\bar{r}}\frac{\partial \bar{n}}{\partial \bar{r}}\right) \tag{7}$$

Following Watson and Wang [31], tangential velocity, $\bar{u}_{\theta}\left(\bar{r},\theta,0\right)=\Omega/\left(1-\beta\,\bar{t}\right)$. Stretching velocity (Li *et al.* [23]) along the radial direction is $\bar{u}_{\bar{r}}\left(\bar{r},\theta,0\right)=\alpha_{c}\,\Omega\,\bar{r}/\left(1-\beta\,\bar{t}\right)$. The initial and boundary conditions are [30]:

$$\left.\begin{aligned}
&\bar{z}=0:\begin{cases}\bar{u}_{\bar{r}}\left(\bar{r},\theta,0\right)=\dfrac{\alpha_{c}\,\Omega\,\bar{r}}{\left(1-\beta\,\bar{t}\right)},\ \bar{u}_{\theta}\left(\bar{r},\theta,0\right)=\dfrac{\Omega\,\bar{r}}{\left(1-\beta\,\bar{t}\right)},\\ \bar{u}_{\bar{z}}\left(\bar{r},\theta,0\right)=\dfrac{-D_{B}}{\left(1-\bar{C}_{w}\right)}\left(\dfrac{\partial \bar{C}}{\partial \bar{z}}\right),\ \bar{T}\left(\bar{r},\theta,0\right)=\bar{T}_{w},\\ -D_{B}\dfrac{\partial \bar{C}}{\partial \bar{z}}=h_{m}\left(\bar{C}_{f}-\bar{C}_{w}\right),\ \bar{n}\left(\bar{r},\theta,0\right)=\bar{n}_{w}\end{cases}\\
&\bar{z}\to\infty:\begin{cases}\bar{u}_{r}\left(\bar{r},\theta,\infty\right)=0,\ \bar{u}_{\theta}\left(\bar{r},\theta,\infty\right)=0,\\ \bar{T}\left(\bar{r},\theta,\infty\right)=\bar{T}_{\infty},\bar{C}\left(\bar{r},\theta,\infty\right)=\bar{C}_{\infty},\\ \bar{n}\left(\bar{r},\theta,\infty\right)=\bar{n}_{\infty}\end{cases}
\end{aligned}\right\} \tag{8}$$

Here Ω ,angular velocity, β , unsteadiness parameter ($\beta\neq 0$) and ($\beta=0$) is associated to steady state, and α_{c} , stretching rate in radial direction.

Following Latiff *et al.* [30], we have adopted the similarity transformations as:

$$\left.\begin{aligned}
&\eta=\sqrt{\frac{\Omega}{\nu}}\frac{\bar{z}}{\sqrt{\left(1-\beta\,\bar{t}\right)}},\ \bar{u}_{\bar{r}}=\frac{\Omega\,\bar{r}}{\left(1-\beta\,\bar{t}\right)}f'\left(\eta\right),\\
&\bar{u}_{\theta}=\frac{\Omega\,\bar{r}}{\left(1-\beta\,\bar{t}\right)}\,g\left(\eta\right),\bar{u}_{\bar{z}}=\frac{-2\sqrt{\Omega\,\nu}}{\sqrt{\left(1-\beta\,\bar{t}\right)}}f\left(\eta\right),\\
&\theta\left(\eta\right)=\frac{\bar{T}-\bar{T}_{\infty}}{\bar{T}_{w}-\bar{T}_{\infty}},\ \phi\left(\eta\right)=\frac{\bar{C}-\bar{C}_{\infty}}{\bar{C}_{f}-\bar{C}_{\infty}},\psi\left(\eta\right)=\frac{\bar{n}}{\bar{n}_{w}}
\end{aligned}\right\} \tag{9}$$

Assimilating the similarity variables (9) into equations (2) – (7) and (8) yields the set of ODEs with boundary conditions as:

$$f'''+2\,f\,f''-f'^{2}+g^{2}-S\left(f'+\frac{1}{2}\eta\,f''\right)=0 \tag{10}$$

$$g''+2\,f\,g'-2\,g\,f'-S\left(g+\frac{1}{2}\eta\,g'\right)=0 \tag{11}$$

$$\theta''+Nb\,\phi'\,\theta'+Nt\,\theta'^{2}-\frac{1}{2}S\,\mathrm{Pr}\,\eta\theta'+2\,\mathrm{Pr}\,f\,\theta'=0 \tag{12}$$

$$\frac{1}{Le\,\mathrm{Pr}}\phi''+\frac{1}{Le\,\mathrm{Pr}}\frac{Nt}{Nb}\theta''-\frac{1}{2}S\,\eta\,\phi'+2\,f\,\phi'=0 \tag{13}$$

$$\frac{1}{Lb\,\mathrm{Pr}}\psi''-\frac{1}{2}S\,\eta\,\psi'+2\,f\,\psi'-Pe\left(\psi\,\phi''+\phi'\,\psi'\right)=0 \tag{14}$$

$$\left.\begin{aligned}
&\eta=0:\begin{cases}f'\left(0\right)=\alpha,\,g\left(0\right)=1,\,f\left(0\right)=\dfrac{f_{w}}{Le\,\mathrm{Pr}}\phi'\left(0\right),\\ \theta\left(0\right)=1,\ \phi'\left(0\right)=Nd\left[1-\phi\left(0\right)\right],\ \psi\left(0\right)=1\end{cases}\\
&\eta\to\infty:\begin{cases}f'\left(\infty\right)=0,g\left(\infty\right)=0,\theta\left(\infty\right)=0,\phi\left(\infty\right)=0,\\ \psi\left(\infty\right)=0\end{cases}
\end{aligned}\right\} \tag{15}$$

Here the time dependent parameter, $S=\beta/\Omega$, Prandtl number, $\Pr=\nu/\alpha$,Brownian motion, $Nb=\tau D_B \Delta C/C_\infty\alpha$, thermophoresis parameter, $Nt=\tau D_T \Delta T/T_\infty\alpha$, Lewis number, $Le=\alpha/D_B$ bio-convection Lewis number, $Lb=\alpha/D_M$ is, bio-convection Peclet number, $Pe=\tilde{b}W_c/\nu$, Stefan blowing parameter, $f_w=\left(\bar{C}_f-\bar{C}_\infty\right)/2\left(1-\bar{C}_w\right)$, Biot number, $Nd=\left(h_m/D_B\right)\sqrt{\nu\left(1-\beta\bar{t}\right)/\Omega}$.

Following the characteristics of engineering coefficients are as follows:

$$\left.\begin{aligned} &Cf_{\bar{r}}=\frac{\tau_{\bar{r}}}{\rho_f\,\bar{u}_{\bar{r}}^2}, Cf_\theta=\frac{\tau_\theta}{\rho_f\,\bar{u}_\theta^2}, Nu_{\bar{r}}=\frac{\bar{r}\,q_w}{k_f\left(\bar{T}_w-\bar{T}_\infty\right)},\\ &Sh_{\bar{r}}=\frac{\bar{r}\,m_w}{D_B\left(\bar{C}_w-\bar{C}_\infty\right)}, Q_{n\bar{r}}=\frac{\bar{r}\,q_n}{D_n\,\bar{n}_w} \end{aligned}\right\} \quad (16)$$

From Eqn. (16), the radial ($\bar{r}$) direction shear stress:

$$\tau_{\bar{r}}=\mu\left(\frac{\partial\bar{u}_{\bar{r}}}{\partial\bar{z}}+\frac{\partial\bar{u}_{\bar{z}}}{\partial\bar{r}}\right)_{\bar{z}=0} \quad (17)$$

Shear stress in tangential (θ) direction:

$$\tau_\theta=\mu\left(\frac{\partial\bar{u}_\theta}{\partial\bar{z}}+\frac{\partial\bar{u}_{\bar{z}}}{\partial\bar{r}}\right)_{\bar{z}=0} \quad (18)$$

Surface heat flux:

$$q_w=-k\left(\frac{\partial\bar{T}}{\partial\bar{z}}\right)_{\bar{z}=0} \quad (19)$$

Surface mass flux:

$$m_w=-D_B\left(\frac{\partial\bar{C}}{\partial\bar{z}}\right)_{\bar{z}=0} \quad (20)$$

Surface motile microorganism flux:

$$q_n=-D_n\left(\frac{\partial\bar{n}}{\partial\bar{z}}\right)_{\bar{z}=0} \quad (21)$$

Introducing Eqns. (9) and (17) -(21) into (16) we get:

$$\left.\begin{aligned} &\sqrt{\frac{\mathrm{Re}_{\bar{r}}}{\left(1-\beta\,\bar{t}\right)}}\;Cf_{\bar{r}}=f'''(0),\\ &\sqrt{\frac{\mathrm{Re}_{\bar{r}}}{\left(1-\beta\,\bar{t}\right)}}\,Cf_\theta=g'(0),\\ &\sqrt{\frac{1}{\mathrm{Re}_{\bar{r}}\left(1-\beta\,\bar{t}\right)}}Nu_{\bar{r}}=-\theta'(0),\\ &\sqrt{\frac{1}{\mathrm{Re}_{\bar{r}}\left(1-\beta\,\bar{t}\right)}}Sh_{\bar{r}}=-\phi'(0),\\ &\sqrt{\frac{1}{\mathrm{Re}_{\bar{r}}\left(1-\beta\,\bar{t}\right)}}Q_{n\bar{r}}=-\psi'(0) \end{aligned}\right\} \quad (22)$$

Here $\mathrm{Re}_{\bar{r}}=\Omega\,\bar{r}^2/\nu$.

3 Adomain decomposition solution of boundary value problem

The higher order coupled ODEs (10)-(14) with boundary conditions (15) does not admit exact analytical solutions. Many such techniques are available for micro and nano-scale flows including finite element techniques [32] and shooting quadrature [33]. Another group of semi-numerical methods has in recent years also become popular. These power-series expansions and using the codes of MAPLE, MATHEMATICA, MATLAB we can compute to numerically. That is (homotopy methods (Daniel and Daniel [34])) and (the successive Taylor series linearization method (STSLM) utilizing Chebyshev interpolating polynomials and Gauss–Lobatto collocation, as employed by Bhatti *et al.* [35]). Finally, Adomian [36] uses a polynomial expansion to get higher accuracy result. Adomian decomposition method (ADM) is employed for nanofluid and multi-physical fluid dynamics problems. ADM is an analytical approximation without using linearization, or perturbation methods. ADM [36] gives an infinite series solution and utilizes recursive relations. The Eqns. (10) -(14) are first rearranged as:

$$f'''=-2\,f\,f''+f'^2-g^2+S\left(f'+\frac{1}{2}\eta\,f''\right) \quad (23)$$

$$g''=-2\,f\,g'+2\,g\,f'+S\left(g+\frac{1}{2}\eta\,g'\right) \quad (24)$$

$$\theta''=-Nb\,\phi'\,\theta'-Nt\,\theta'^2+\frac{1}{2}S\,\Pr\,\eta\,\theta'-2\,\Pr\,f\,\theta' \quad (25)$$

$$\phi''=-\frac{Nt}{Nb}\theta''+\frac{1}{2}Le\,\Pr\,S\,\eta\,\phi'-2\,Le\,\Pr\,f\,\phi' \quad (26)$$

$$\psi''=\frac{1}{2}Le\,\Pr\,S\,\eta\,\psi'-2\,Lb\,\Pr\,f\,\psi'+Lb\,\Pr\,Pe\left(\psi\,\phi''+\phi'\,\psi'\right) \quad (27)$$

Applying ADM, we introduce

$L_1=\dfrac{d^3}{d\eta^3}()$ and $L_2=\dfrac{d^2}{d\eta^2}()$ with inverse operators

$L_1^{-1}()=\int_0^\eta\int_0^\eta\int_0^\eta()d\eta d\eta d\eta$ and $L_2^{-1}()=\int_0^\eta\int_0^\eta()d\eta d\eta.$

Thus Eqns. (23) - (27) become:

$$L_1^{-1}\left(L_1 f\right) = -2\,L_1^{-1}\left(f\ f''\right) + L_1^{-1}\left(f'^2\right) - L_1^{-1}\left(g^2\right) + S\,L_1^{-1}\left(f' + \frac{1}{2}\eta\ f''\right) \tag{28}$$

$$L_2^{-1}\left(L_2 g\right) = -2\,L_2^{-1}\left(f\ g'\right) + 2\,L_2^{-1}\left(g\ f'\right) + S\,L_2^{-1}\left(g + \frac{1}{2}\eta\ g'\right) \tag{29}$$

$$L_2^{-1}\left(L_2\,\theta\right) = -Nb\,L_2^{-1}\left(\phi\,\theta'\right) - Nt\ L_2^{-1}\left(\theta'^2\right) + \frac{1}{2}S\ \mathrm{Pr}\,L_2^{-1}\left(\eta\,\theta'\right) - 2\,\mathrm{Pr}\,L_2^{-1}\left(f\ \theta'\right) \tag{30}$$

$$L_2^{-1}\left(L_2\,\phi\right) = -\frac{Nt}{Nb}L_2^{-1}\left(\theta''\right) - \frac{1}{2}Le\,\mathrm{Pr}\,S\ L_2^{-1}\left(\eta\,\phi'\right) - 2\,Le\,\mathrm{Pr}\,L_2^{-1}\left(f\ \phi'\right) \tag{31}$$

$$L_2^{-1}\left(L_2\,\psi\right) = -\frac{1}{2}Le\,\mathrm{Pr}\,S\,L_2^{-1}\left(\eta\,\psi'\right) - 2\,Lb\,\mathrm{Pr}\ L_2^{-1}\left(f\ \psi'\right) + Lb\,\mathrm{Pr}\,Pe\,L_2^{-1}\left(\psi\,\phi'' + \phi'\psi'\right) \tag{32}$$

The unknown functions $f(\eta), g(\eta), \theta(\eta), \phi(\eta)$ and $\psi(\eta)$ can be expressed as infinite series of the form:

$$\left.\begin{aligned} f(\eta) &= \sum_{m=0}^{\infty} f_m,\ g(\eta) = \sum_{m=0}^{\infty} g_m,\ \theta(\eta) = \sum_{m=0}^{\infty} \theta_m, \\ \phi(\eta) &= \sum_{m=0}^{\infty} \phi_m,\ \psi(\eta) = \sum_{m=0}^{\infty} \psi_m \end{aligned}\right\} \tag{33}$$

The remaining terms of (28) -(32) can be expressed as:

$$\left.\begin{aligned} &\sum_{m=0}^{\infty} A_m = f\ f'',\ \sum_{m=0}^{\infty} B_m = f'^2, \\ &\sum_{m=0}^{\infty} C_m = g^2,\ \sum_{m=0}^{\infty} D_m = f', \\ &\sum_{m=0}^{\infty} E_m = f'',\ \sum_{m=0}^{\infty} F_m = f\ g', \\ &\sum_{m=0}^{\infty} G_m = f'\,g,\ \sum_{m=0}^{\infty} H_m = g, \\ &\sum_{m=0}^{\infty} I_m = g',\ \sum_{m=0}^{\infty} J_m = \theta'\,\phi', \\ &\sum_{m=0}^{\infty} K_m = \theta'^2,\ \sum_{m=0}^{\infty} L_m = \theta', \\ &\sum_{m=0}^{\infty} M_m = f\ \theta',\ \sum_{m=0}^{\infty} N_m = \theta'', \\ &\sum_{m=0}^{\infty} O_m = \phi',\ \sum_{m=0}^{\infty} P_m = f\ \phi', \\ &\sum_{m=0}^{\infty} Q_m = \psi',\ \sum_{m=0}^{\infty} R_m = f\ \psi', \\ &\sum_{m=0}^{\infty} S_m = \psi\ \phi'',\ \sum_{m=0}^{\infty} T_m = \phi'\,\psi' \end{aligned}\right\} \tag{34}$$

Here recursive formula is used to find all the components. The exact solutions of (23) -(27) are

$$\left.\begin{aligned} f(\eta) &= Lim \sum_{m=0}^{\infty} f_m,\ g(\eta) = Lim \sum_{m=0}^{\infty} g_m, \\ \theta(\eta) &= Lim \sum_{m=0}^{\infty} \theta_m,\ \phi(\eta) = Lim \sum_{m=0}^{\infty} \phi_m, \\ \psi(\eta) &= Lim \sum_{m=0}^{\infty} \psi_m \end{aligned}\right\} \tag{35}$$

Therefore, the RHSs of Eqns. (28) - (32) can be written as:

$$L_1^{-1}\left(L_1 f\right) = f(\eta) - f(0) - \eta\ f'(0) - \frac{\eta^2}{2!}f''(0) \tag{36}$$

$$L_2^{-1}\left(L_2 g\right) = g(\eta) - g(0) - \eta\,g'(\eta) \tag{37}$$

$$L_2^{-1}\left(L_2\theta\right) = \theta(\eta) - \theta(0) - \eta\,\theta'(0) \tag{38}$$

$$L_2^{-1}\left(L_2\phi\right) = \phi(\eta) - \phi(0) - \eta\,\phi'(0) \tag{39}$$

$$L_2^{-1}\left(L_2\psi\right) = \psi(\eta) - \psi(0) - \eta\,\psi'(0) \tag{40}$$

From (15), invoking the boundary conditions:

$$\left.\begin{aligned} &f(0) = -\beta(1-r),\ f'(0) = \alpha, \\ &f''(0) = p,\ g(0) = 1,\ g'(0) = q, \\ &\theta(0) = 1,\ \theta'(0) = t,\ \phi(0) = r, \\ &\phi'(0) = -Nd(1-r),\ \psi(0) = 1, \\ &\psi'(0) = u \end{aligned}\right\} \tag{41}$$

The solutions of Eqns. (23) - (27) may therefore be written as

$$f(\eta) = -\beta(1-r) + \eta\alpha + \frac{\eta^2}{2}p - 2\,L_1^{-1}\left(f\ f''\right) + L_1^{-1}\left(f'^2\right) - L_1^{-1}\left(g^2\right) + S\,L_1^{-1}\left(f' + \frac{1}{2}\eta\ f''\right) \tag{42}$$

$$g(\eta) = 1 + \eta\,q - 2\,L_2^{-1}\left(f\ g'\right) + 2\,L_2^{-1}\left(g\ f'\right) + S\,L_2^{-1}\left(g + \frac{1}{2}\eta\ g'\right) \tag{43}$$

$$\theta(\eta) = 1 + \eta\,t - Nb\,L_2^{-1}\left(\phi'\,\theta'\right) - Nt\,L_2^{-1}\left(\theta'^2\right) + \frac{1}{2}S\,\mathrm{Pr}\,L_2^{-1}\left(\eta\,\theta'\right) - 2\,\mathrm{Pr}\,L_2^{-1}\left(f\ \theta'\right) \tag{44}$$

$$\phi(\eta) = r - Nd(1-r)\eta - \frac{Nt}{Nb}L_2^{-1}\left(\theta''\right) + \frac{1}{2}Le\,\mathrm{Pr}\,S\,L_2^{-1}\left(\eta\,\phi'\right) - 2\,Le\,\mathrm{Pr}\,L_2^{-1}\left(f\ \phi'\right) \tag{45}$$

$$\psi(\eta)=1+u\,\eta+\frac{1}{2}Le\,\mathrm{Pr}\,S\,L_2^{-1}(\eta\,\psi')-2\,Lb\,\mathrm{Pr}\,L_2^{-1}(f\,\psi')+Lb\,\mathrm{Pr}\,Pe\,L_2^{-1}(\psi\,\phi''+\phi'\psi') \tag{46}$$

Here it is necessary to evaluate the unknowns *p*, *q* ,*r*, *t*, *u*. Utilizing Eqns. (42) - (46) the initial imposed solutions along with higher order recursive solutions are

$$f_0(\eta)=-\beta(1-r)+\eta\alpha+\frac{\eta^2}{2}p \tag{47}$$

$$g_0(\eta)=1+\eta\,q \tag{48}$$

$$\theta_0(\eta)=1+\eta\,t \tag{49}$$

$$\phi_0(\eta)=r-Nd\,(1-r)\eta \tag{50}$$

$$\psi_0(\eta)=1+u\,\eta \tag{51}$$

and

$$f_{m+1}=-2\,L_1^{-1}(f\,f'')+L_1^{-1}(f'^2)-L_1^{-1}(g^2)+S\,L_1^{-1}\left(f'+\frac{1}{2}\eta\,f''\right) \tag{52}$$

$$g_{m+1}=-2\,L_2^{-1}(f\,g')+2L_2^{-1}(g\,f')+S\,L_2^{-1}\left(g+\frac{1}{2}\eta\,g'\right) \tag{53}$$

$$\theta_{m+1}=-Nb\,L_2^{-1}(\phi'\,\theta')-Nt\,L_2^{-1}(\theta'^2)+\frac{1}{2}S\,\mathrm{Pr}\,L_2^{-1}(\eta\,\theta')-2\,\mathrm{Pr}\,L_2^{-1}(f\,\theta') \tag{54}$$

$$\phi_{m+1}=-\frac{Nt}{Nb}L_2^{-1}(\theta'')+\frac{1}{2}Le\,\mathrm{Pr}\,S\,L_2^{-1}(\eta\,\phi')-2\,Le\,\mathrm{Pr}\,L_2^{-1}(f\,\phi') \tag{55}$$

$$\psi_{m+1}=\frac{1}{2}Le\,\mathrm{Pr}\,S\,L_2^{-1}(\eta\,\psi')-2\,Lb\,\mathrm{Pr}\,L_2^{-1}(f'\psi')+Lb\,\mathrm{Pr}\,Pe\,L_2^{-1}(\psi\,\phi''+\phi'\,\psi') \tag{56}$$

Using *m=0,1,2* in Eqns. (52) -(56) with the aid of (34) the solutions of Eqns. (23) -(27) expressed in (33) emerge as follows:

$$f(\eta)=-\beta(1-r)+\eta\alpha+\frac{\eta^2}{2}p+T_1\eta^3+(T_2+T_7)\eta^4+(T_3+T_8+T_{17})\eta^5+(T_9+T_{18})\eta^6+(T_{10}+T_{19})\eta^7+(T_{11}+T_{20})\eta^8+T_{21}\eta^9+T_{22}\eta^{10}+T_{23}\eta^{11} \tag{57}$$

$$g(\eta)=1+\eta\,q+T_4\,\eta^2+(T_5+T_{12})\eta^3+(T_6+T_{13}+T_{24})\eta^4+(T_{14}+T_{25})\eta^5+(T_{16}+T_{27})\eta^7+T_{28}\eta^8+T_{29}\eta^9+T_{30}\eta^{10}+T_{31}\eta^{11} \tag{58}$$

$$\theta(\eta)=1+\eta\,t+T_{32}\,\eta^2+(T_{33}+T_{41}+T_{59})\eta^3+(T_{34}+T_{42}+T_{60})\eta^4+(T_{43}+T_{61})\eta^5+(T_{44}+T_{62})\eta^6+(T_{45}+T_{63})\eta^7+T_{64}\eta^8+T_{65}\eta^9+T_{66}\eta^{10} \tag{59}$$

$$\phi(\eta)=r-Nd(1-r)\eta+(T_{35}+T_{46})\eta^2+(T_{36}+T_{47}+T_{67})\eta^3+(T_{37}+T_{48}+T_{68})\eta^4+(T_{49}+T_{69})\eta^5+(T_{50}+T_{70})\eta^6+(T_{51}+T_{71})\eta^7+T_{72}\,\eta^8+T_{73}\,\eta^9+T_{74}\,\eta^{11} \tag{60}$$

$$\psi(\eta)=1+u\,\eta+T_{52}\,\eta+(T_{38}+T_{53}+T_{75})\eta^2+(T_{39}+T_{54}+T_{76})\eta^3+(T_{40}+T_{55}+T_{77})\eta^4+(T_{56}+T_{78})\eta^5+(T_{57}+T_{79})\eta^6+(T_{58}+T_{80})\eta^7+T_{81}\eta^8+T_{82}\eta^9+T_{83}\eta^{10} \tag{61}$$

The values of the notations $T_i's, i=1-83$ are summarized in the Appendix.

4 Validation of ADM solutions

The assumed values $f''(0)=p, g'(0)=q, \phi(0)=r,$ $\theta'(0)=t$ and $\psi'(0)=u$ are calculated by using symbolic software MATLAB [39] with code bvp4c. The conformity of ADM with earlier , the work of Latiff *et al.* [30] those are used Runge-Kutta quadrature rule. In presence of unsteadiness parameter, *S* (*S* < 0) various cases are taken care of such as, a *non-deformable disk* (α = 0) and a *radially stretching disk* (α = 1.0). These values are presented in **Tables 1 and 2** for the radial local skin friction $f''(0)$, local circumferential skin friction $g'(0)$,local Nusselt number $-\theta'(0)$, local Sherwood number or nano-particle wall concentration gradient $-\phi'(0)$ and motile micro-organism wall mass flux $-\psi'(0)$ i.e. number density gradient function). The confidence of ADM is justified due to good correlation.

Table-1: Comparison of results when $\alpha = 0$

S	$f''(0)$		$g'(0)$	
	RK45	**ADM** (present)	**RK45**	**ADM** (present)
-0.1	0.5287	0.527889	-0.5779	-0.57663
-0.2	0.5496	0.549070	-0.5407	-0.53914
-0.5	0.6132	0.613551	-0.4280	-0.42734
-1	0.7196	0.719461	-0.2365	-0.23433
-2	0.9315	1.079269	0.1550	0.282443

S	$-\theta'(0)$	$-\phi'(0)$	$-\psi'(0)$
-0.1	0.38045	0.107966	0.444195
-0.2	0.412973	0.107892	0.476487
-0.5	0.499995	0.112086	0.564525
-1	0.616827	0.12128	0.683967
-2	0.826726	0.136449	0.897399

Table-2: Comparison of results when $\alpha = 1.0$

S	$f''(0)$		$g'(0)$	
	RK45	**ADM** (present)	**RK45**	**ADM** (present)
-0.1	-0.9191	-0.91796	-1.4656	-1.4604
-0.2	-0.8896	-0.88725	-1.4441	-1.43743
-0.5	-0.8008	-0.79244	-1.3797	-1.36755
-1	-0.6520	-0.62533	-1.2716	-1.24843
-2	-0.3517	-0.31715	-1.0534	-0.93917

S	$-\theta'(0)$	$-\phi'(0)$	$-\psi'(0)$
-0.1	0.722863	0.089094	0.775458
-0.2	0.746844	0.092758	0.80035
-0.5	0.812721	0.102231	0.868371
-1	0.907939	0.113936	0.966593
-2	1.055982	0.126582	1.117173

5 ADM results and interpretation

Selected ADM solutions for $f'(\eta), g(\eta), \theta(\eta), \phi(\eta), \psi(\eta), f''(0), g'(0), -\theta'(0), -\phi'(0)$ and $-\psi'(0)$ are given. For brevity our discussion restricted to the influences of stretching (S), unsteadiness (α), and Stefan blowing/suction (f_w). At the time of computation, we have considered as $Nd = 0.4, Nb = Nt = 10^{-7}, Le = Lb = Pe = 1, \alpha = 0.2, \Pr = 0.7$. These corresponds to air-based nanofluid with weak Brownian motion, thermophoresis and equal nano-particle, micro-organisms and thermal diffusivities. The current simulations apply to air-based rotating bio-nano rotating disk flows. (Pr = 0.7 for the base fluid of air). The data selected for nanofluid properties is based on the best currently available, namely the Das *et al.* [16] reference is based on real experiments.

Results are visualized in **Figures 2-16** and **Tables 3-4**.

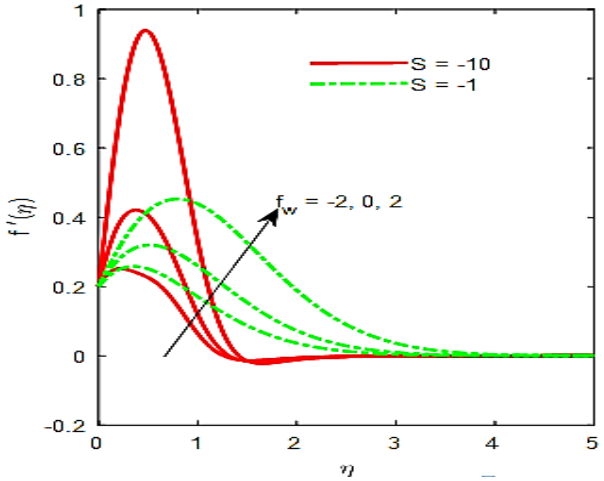

Figure 2 Suction/injection and unsteadiness parameters effect on radial velocity.

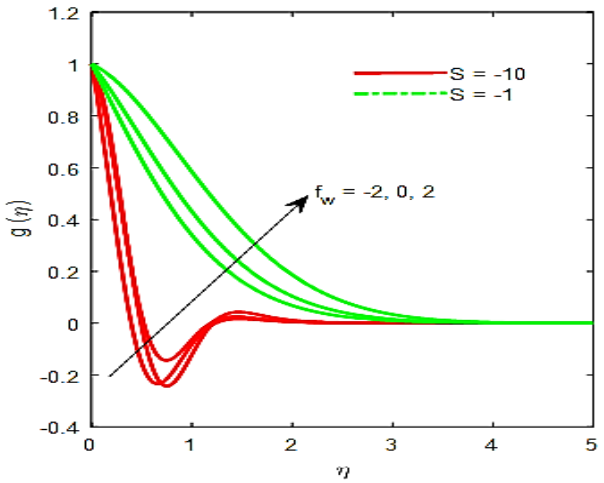

Figure 3 Suction/injection and unsteadiness parameters effect on circumferential velocity.

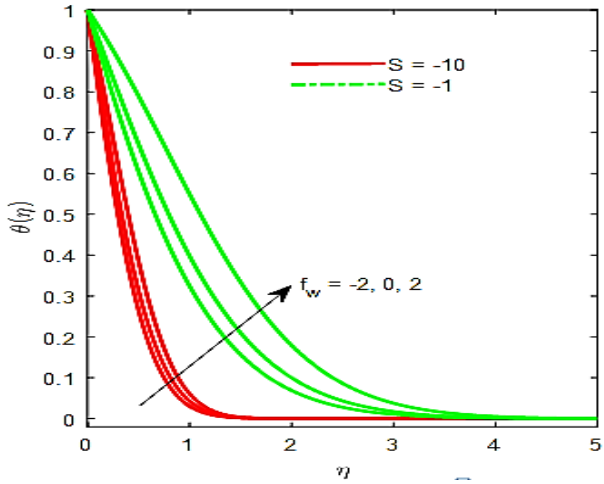

Figure 4 Suction/injection and unsteadiness parameters effect on temperature.

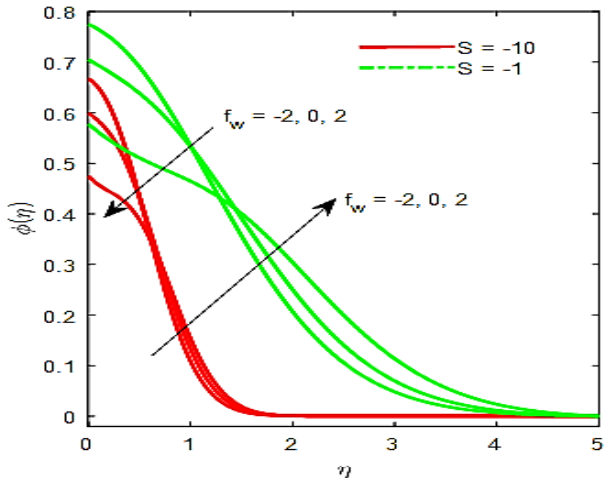

Figure 5 Suction/injection and unsteadiness parameters effect on concentration.

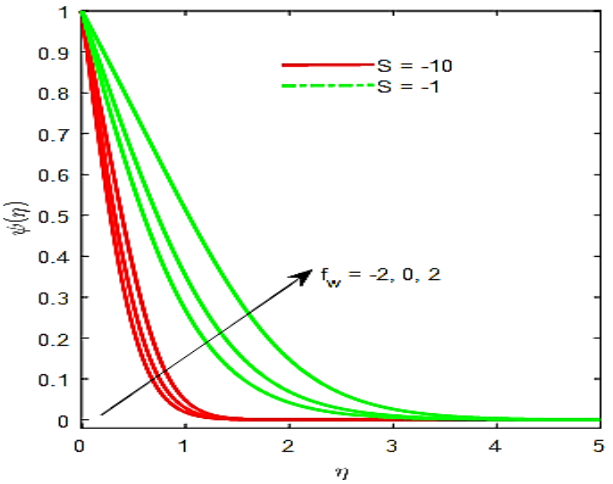

Figure 6 Suction/injection and unsteadiness parameter effect on motile microorganism

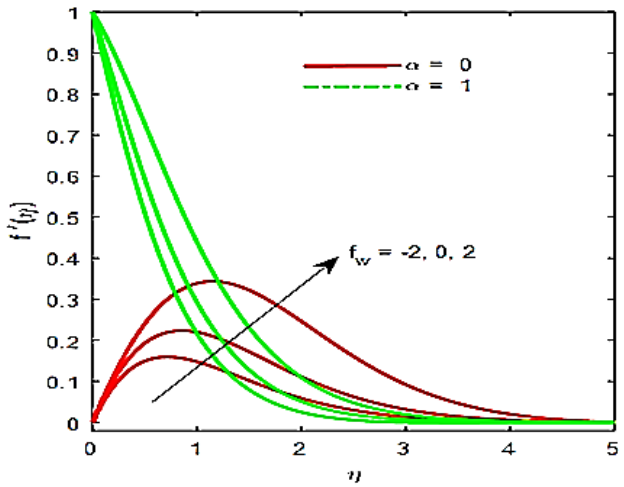

Figure 7 Suction/injection and disk stretching parameters effect on radial velocity.

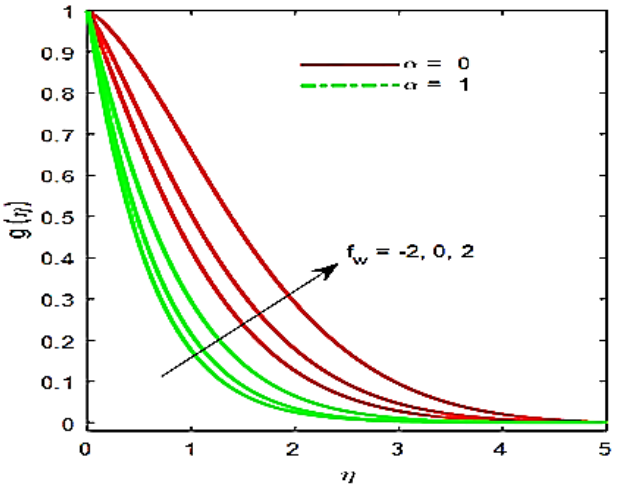

Figure 8 Suction/injection and disk stretching parameters effect on circumferential velocity.

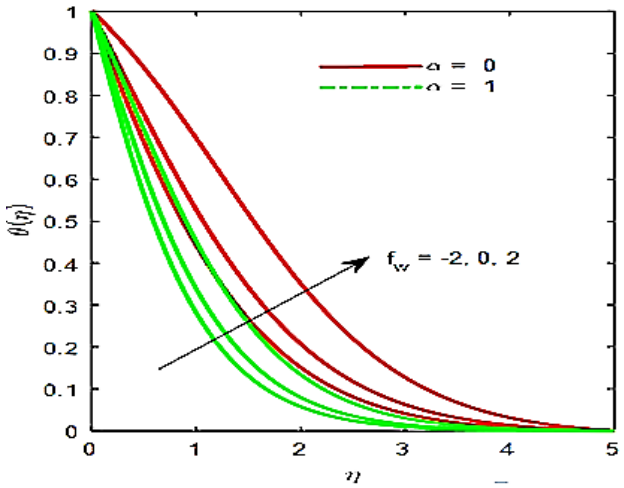

Figure 9 Suction/injection and disk stretching parameters effect on temperature.

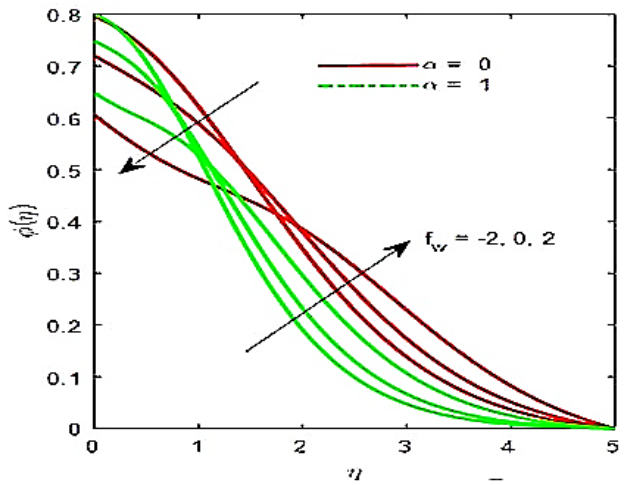

Figure 10 Suction/injection and disk stretching parameters effect on nanoparticle concentration

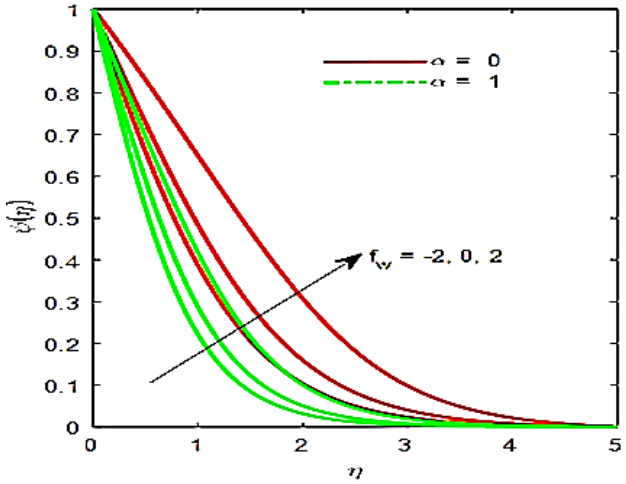

Figure 11 Suction/injection and disk stretching parameters effect on motile microorganism.

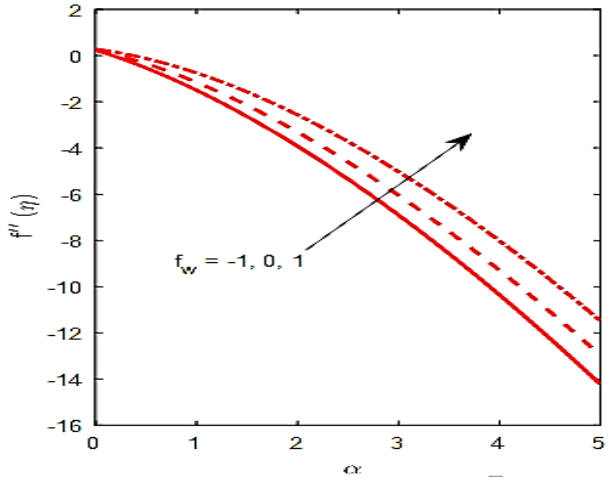

Figure 12 Suction/injection parameter effect on radial skin friction.

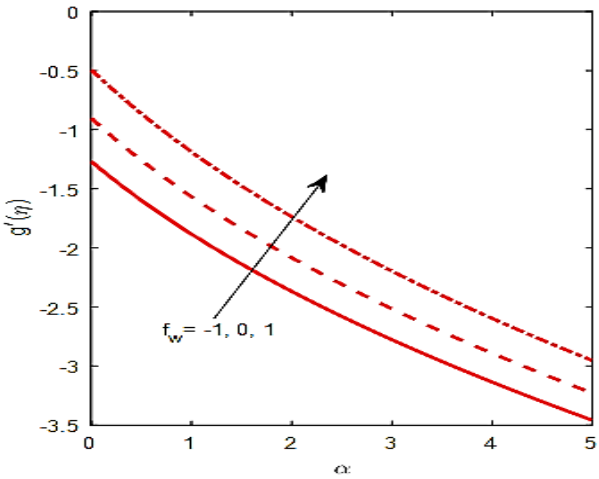

Figure 13 Suction/injection parameter effect on Azimuthal skin friction.

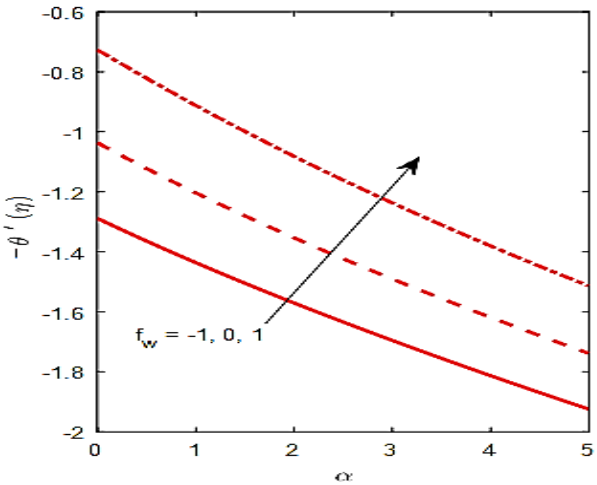

Figure 14 Suction/injection parameter effect on Nusselt number .

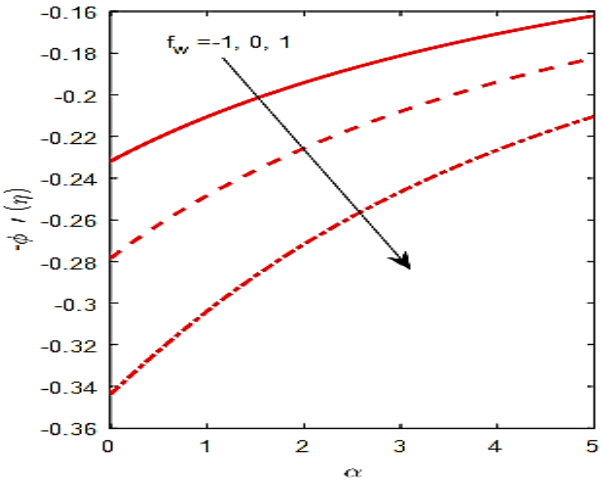

Figure 15 Suction/injection parameter effect on Sherwood number.

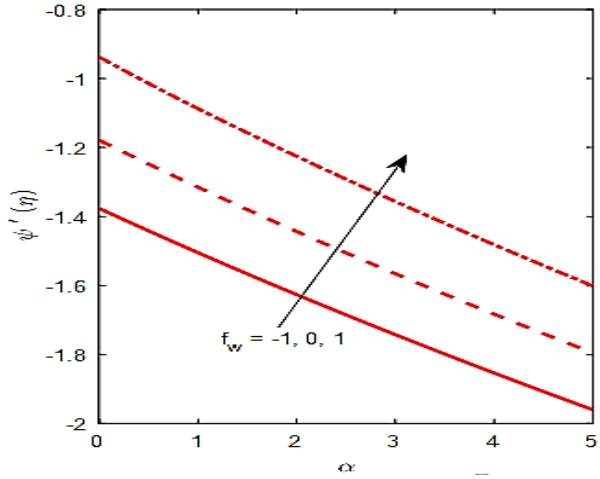

Figure 16 Suction/injection parameter effect on microorganism wall mass flux.

Latiff *et al.* [30] rapt principally on the influence of the radial stretching parameter (α) and to a lesser extent on the unsteadiness parameter (*S*). Herein we address both and consider significantly stronger blowing effects. Figures 2- 6 illustrate the collective influence of unsteadiness parameter (*S*) and Stefan blowing/suction (f_w) on radial velocity, circumferential velocity, temperature, nano -particle concentration and motile microorganism density number. It is important to note that suction is not generated by perforations at the disk surface. The suction effect (reverse Stefan blowing) is associated with mass flux from the free stream of the boundary layer to the rotating disk surface. Similarly, the Stefan blowing is caused by the mass flux from rotating disk surface to the free stream. Additionally, it is pertinent to mention that weak radial disk stretching is prescribed (α=0.2). Figure 2 clearly shows that with strong suction ($f_w < 0$) radial flow deceleration is induced whereas very strong radial flow acceleration is generated with strong blowing ($f_w > 0$). The swirling flow mobilized by the disk rotation acts as a pump drawing fluid inward which spreads radially outwards over the disk face. This assists in momentum development in the radial direction. The presence of suction causes adherence of the boundary layer to disk surface whereas blowing results in the opposite effect. With weak unsteadiness (*S*=-1) i.e. *weak disk deceleration*, there is a more gradual evolution in radial velocity profiles from the disk surface ($\eta = 0$) to the free stream than for strong disk deceleration (*S* = -10). A very strong overshoot arises for the case of strong disk deceleration with strong blowing (*S* = -10, f_w =2). This generates the maximum radial velocity. With absence of suction or blowing the peak is reduced and displaced closer to the wall and is in fact almost eliminated with suction (*S* = -10, f_w =2). For the weak disk deceleration case (S = -1) a similar effect is produced although peak radial velocity magnitudes are somewhat lower. Negative radial velocity (back flow) is only induced for a short zone further from the disk surface with strong deceleration. The smoothness of the profile confirms the convergence of the ADM solutions for infinite boundary conditions imposed herewith. Figure 3 depicts the evolution in circumferential (azimuthal) velocity with transverse coordinate and various deceleration i.e. unsteadiness (*S*) and blowing/suction (f_w) parameters. There is a distinct absence of velocity overshoots for any combination of parameters. With *weak disk deceleration* the circumferential velocity decays monotonically from the disk surface to the free stream, whether suction or blowing is present. However, with strong disk deceleration, there is a much sharper decay in circumferential velocity from the disk surface resulting in backflow nearby disk. However, beside further progression into boundary layer there is a re-surge in circumferential velocity which eventually vanishes in the free stream. The circumferential (and radial velocity) distributions are generally also consistent with numerous other Von Kármán swirling flow studies, notably Evans [40]who did not consider disk *deceleration*) and more recently Fang and Tao [41] Watson and Wang [31]. Furthermore, the presence of nano-particles and micro-organisms therefore does not dramatically alter the classical velocity distributions in Von Kármán swirling flow. Figure 4 depicts the response in temperature distribution to unsteadiness (*S*) and Stefan blowing/suction (f_w) effects. Substantially lower values are computed with strong disk deceleration (*S*= -10) compared with weak disk acceleration (*S* = -1) indicating that thinner thermal boundary layer. As anticipated the temperatures are enhanced with Stefan blowing whereas they are reduced with suction. Additionally, there is a greater spread profiles at weaker deceleration compared with stronger deceleration. The diffusion of heat energy in the boundary layer dominion is clearly impacted with retardation in the disk spin and mass transfer conditions. Even though the regime is forced convection and there are no buoyancy effects, there is still significant coupling of the radial momentum (10) and energy equation (12) via the term $2\,\mathrm{Pr}\, f\,\theta'$ in the latter. The unsteadiness parameter (*S*) also appears in many terms in all the conservation equations, notably in the radial equation in the term $-S\left(f' + (1/2)\eta\, f''\right)$, in the azimuthal equation in the term $-S\left(g + (1/2)\eta\, g'\right)$ and in the energy equation in the term $-(1/2)S\,Pr\,\eta\theta'$. The momenta and temperature fields are therefore very sensitive to adjustment in the unsteadiness parameter and this is reflected in figures 2-4. A further point of note is that in figures 2-4 there is never any intersection of profiles corresponding to a specific unsteadiness value with each other. This trend is not sustained in Figure 5 displays the influence of unsteadiness and blowing/suction parameter on nano-particle concentration profiles. In addition to that the profile is partitioned into two distinct layer such as disk region (near and far). In the first region i.e. $0 < \eta < 1$, for strong gust the magnitude of concentration layer is elevated and has a dominating

role for weak disk deceleration $(S=-1)$ in comparison with strong disk deceleration $(S=-10)$. Further, in the second region the effect is opposite i.e. concentration reduces with an increase in blowing whereas suction slightly enhances it. Again, the profiles deviate for particular value of *S* when we compare the weak situation with strong situation of disk deceleration. In the present case we have not discussed the case of $S > 0$. It validates with the mathematical expression presented in eqn. (13) $-(1/2)S\eta\phi'$ and moreover at the time of computation via coupling terms, $2f\phi'$. Figure 6 exhibits the effects of unsteadiness and Stefan blowing/suction on motile micro-organism density profiles for fixed values of various pertinent parameters. Detected that, an increase in blowing inflate micro-organisms effect is reversed in case of suction. Motile micro-organism retards significantly with Strong deceleration in comparison with weak disk deceleration. It is also clear from the expression presented in eqn. (14) $-(1/2)S\eta\psi'$ that Micro-organism suppressed directly and via coupling term $2f\psi'$. Also, notable that there is a hefty mix between the nano-particle species (ϕ) and micro-organism species (ψ) field via the terms, $-Pe(\psi\phi''+\phi'\psi')$.

Figures 7-11 illustrate the radial velocity, circumferential velocity, temperature, nano-particle concentration and motile micro-organism for various α and f_w. A further motivation for the current study was to elaborate in more detail the findings of Latiff *et al.* [30] which were limited in interpretation. Radial velocity (figure 7) is accentuated with disk stretching i.e. the radial flow is strongly accelerated. However, this is confined to the near-wall zone. The profiles with disk stretching present and absent $(\alpha=0)$ are significantly different. For $\alpha>0$ the velocity at the surface is non-zero which is presented in eqn. (15). Therefore, the traditional no-slip condition is modified with the particular type of slip condition and suggests decaying in the boundary layer. When $\alpha=0$, Von Kármán [9] presented their problem with classical no-slip radial velocity boundary condition. This results in the characteristic growth of the radial velocity from zero at the wall to a near-wall peak and subsequent decay into the free stream. In the disk stretching case, Stefan blowing consistently accelerates the radial flow whereas suction decelerates the flow up to considerably large distances from the disk surface; eventually all profiles converge asymptotically to vanishing radial velocity in free stream. In the non-deformable disk case higher radial velocities are achieved further from the disk surface compared with the stretching case; again, all distributions converge to zero in the free stream. Figure 8 depicts evolution in azimuthal velocity distribution with transverse coordinate, for the case of disk deceleration (*S* = -0.5). In all cases decay from the wall to the free stream is maintained. Stretching effect therefore does not influence the topology of circumferential velocity distributions since the parameter α does not arise in the circumferential velocity disk surface (wall) boundary condition in Eqn. (15). However lower circumferential velocity magnitudes are evidently induced with disk stretching. This is attributable to the re-distribution in momentum and the coupling of the radial and azimuthal (circumferential) momentum Eqns. (10) and (11) via the terms $+g^2$ in the former and $2fg', -2gf'$ in the latter. The boost in radial momentum near the disk surface is balanced by depletion in azimuthal momentum, since momentum has to be conserved. The azimuthal flow which is a secondary flow is therefore depleted, which is a predictable quality of swirling flows and studied by many including Shevchuk [11], for macroscopic fluids and by Turkyilmazoglu [17] for nanofluids. With strong Stefan blowing the circumferential flow is decelerated owing to assisting momentum development whereas with strong suction it is retarded, irrespective of whether the disk is stretching or not. This pattern is sustained throughout the entire boundary layer regime. Figure 9 illustrates the modification in temperature distribution with the combined effects of blowing/suction parameter (f_w) and radial stretching parameter (α). A similar response is computed as with the azimuthal velocity field. Disk stretching is found to reduce temperatures (and thermal boundary layer thickness) whereas without stretching higher temperatures are generated in the boundary layer. The Prandtl number Pr is set as 0.7 (air). Since this parameter represents the ratio of momentum diffusion to thermal diffusion, the latter exceeds the former. This results in greater heat transfer to the disk surface from the body of the nanofluid which manifests in a reduction in temperatures. The disk stretching enhances the radial flow but curtails the azimuthal flow. Therefore, while momentum diffuses faster in the radial field which accelerates the radial flow, this impedes thermal diffusion from the disk surface. Strong blowing however enhances temperatures whereas strong suction decreases them, and this is generally, enforced whether the disk is stretching or

not. Figure 10 illustrates the nano-particle concentration profiles for various blowing/suction parameter (f_w) and radial stretching parameter (α) values. Significant inter-twining of profiles is observed. With disk stretching and strong Stefan blowing ($f_w = 2$) initially the nano-particle concentrations are greater in the vicinity of the disk. Suction ($f_w = -2$) is observed to reduce magnitudes in this zone. However further from the wall the absence of disk stretching ($\alpha = 0$) results in enhanced nano-particle concentrations (volume fractions) and furthermore suction is found to boost magnitudes. The nano-particle concentration boundary layer thickness therefore does not exhibit a consistent response to disk stretching or mass transfer effects. Micro-organism density retards with disk stretching whereas in the absence of disk stretching it enhances (Figure 11). The thickness of both the boundary layer for micro-organism density and micro-organism species with greater Stefan blowing consistently since the diffusivity of Micro-organism species and nano-particle species equal to momentum diffusivity in Figures 10 and 11.

Figures 12-16 show the variation of different mass transfer parameters (f_w) for α = 0 on the physical quantities of interest described earlier in eqns. (17)-(21). It is seen that $f''(0)$ decreases as an increase in α (Figure 12). From Figure 13, Azimuthal skin friction $g'(0)$, too diminish with increasing α although upend profiles are computed as compared with $f''(0)$. However, in case of blowing azimuthal skin friction is higher as compared to suction. For the non-deformable disk (α = 0), both figures 12 and 13 radial and azimuthal skin friction are maximum. Figure 14 describes the rate of heat transfer ($-\theta'(0)$) for various disk stretching. Fall in Nusselt number is marked with an increasing disk stretching. It is due to the reason, as increase in stretching in disk thermal diffusion decreases from the boundary layer to the wall. As a result, an increase in suction heat transfer rates retards. Figure 15 displays the Sherwood number which is opposite to that of fluid temperature. Though diffusion of nano-particles is greater which boosts Sherwood number as stretching increases. With no stretching mass transfer rate is minimized and effect is reversed for higher stretching ($\alpha = 5$). However, gust is favorable to reduce Sherwood number whereas suction enhances it. Finally, Figure16 illustrates the influence of suction or blowing on motile micro-organism wall flux in presence or absence of stretching. The inter-connection is linear between motile micro-organism wall flux and disk stretching rate. In case of $\alpha = 0$ the magnitude is maximum than that of $\alpha = 5$. An increase in f_w clearly boosts the $-\psi'(0)$ for all values of the α. Conversely with strong suction there is a decrease in $-\psi'(0)$.

Tables 3 and 4 also show the response in $f''(0)$, $g'(0)$, $-\theta'(0)$, $-\phi'(0)$ and $-\psi'(0)$ to a collective variation in respectively, unsteadiness parameter (S) and mass transfer parameter (f_w) and stretching rate parameter (α) and mass transfer parameter (f_w). Table 4 has already been elaborated via Figures 12-16 and is provided as a benchmark for reader interested in extending the current study. Table 3 shows that with strong disk deceleration, radial skin friction is increased when suction is present whereas it is more dramatically elevated with Stefan blowing. Azimuthal skin friction is however very strongly reduced with disk deceleration and suction and weakly depleted with Stefan blowing. Similarly, $-\theta'(0)$, $-\phi'(0)$ and $-\psi'(0)$ are all reduced more substantially with disk deceleration and suction than with disk deceleration and Stefan blowing.

Table-3: Values of p,q,t,r and u for $Lb=Le=Pe=1, Nt=Nb=10^{-7}, Nd=0.4, \alpha=0.2$ and $\Pr=0.7$

S	f_w	p	q	t	r	u
-10	-2	0.5596	-2.104903	-1.929682	-0.132956	-1.957172
-10	0	1.257078	-0.895418	-1.606009	-0.159922	-1.667821
-10	2	2.609129	-0.630569	-1.1918845	-0.2100199	-1.3196154
-1	-2	0.3653548	-0.752887	-0.8893799	-0.089496	-0.9295347
-1	0	0.5044829	-0.4913227	-0.677455	-0.1178999	-0.7418018
-1	2	0.6159968	-0.1811816	-0.3668128	-0.1689003	-0.4682837

Table-4: Values of p,q,t,r and u for $Lb=Le=Pe=1, Nt=Nb=10^{-7}, Nd=0.4, S=-1$ and $\Pr=0.7$

α	f_w	p	q	t	r	u
0	-2	0.5528668	-0.6447907	-0.6845458	-0.0814359	-0.7254309
0	0	0.6127437	-0.4283855	-0.4997283	-0.1120909	-0.5642468
0	2	0.61156458	-0.1530077	-0.2328863	-0.1578918	-0.3177025
1	-2	-1.0925267	-1.6093531	-1.0039318	-0.0800487	-1.04140008
1	0	-0.8008664	-1.380858	-0.8102526	-0.1006629	-0.8647324
1	2	-0.4101898	-1.0504819	-0.5239979	-0.1405089	-0.6126271

6 Conclusions

3-dimensional laminar viscous gyrotactic forced bioconvection in swirling dilute nanofluid unsteady mathematical model flow from a rotating disk configuration with convective mass boundary conditions and Stefan blowing. Radial stretching of the disk has been included. The model is inspired by novel developments in nanofluid rotating bio-reactors exploiting specific taxes of thermophile microganisms. Employing the Buongiorno formulation and the Fang-Tao transformations [41], the normalized boundary layer equations for mass, radial and azmiuthal (circumferential) momentum, heat (energy), micro-organism density and nano-particle concentration function derived subject to physically viable wall (disk surface) and free stream boundary conditions. The Adomian decomposition method (ADM) has been implemented with MATLAB symbolic software to solve the emerging high order nonlinear coupled ordinary differential boundary value problem. Verification of solutions has also been included with alidation with earlier Runge-Kutta shooting quadrature solutions [30]. The present analysis has shown that:

- An Increase in stretching parameter alog the radial direction decreases all the engineerig coefficients except local Sherwood number of nanoparticles.
- Thinning in thermal boundary layer is marked due to disk deceleration which accelerates radial flow.
- Radial and azimuthal flow along with nanoparticle concentration enhances with an increase in Stefan blowing however, suction causes a reverse effect.
- An increasein suction is favorable to enhance the local Sherwood number whereas other coefficients. Futher, other physical quantuities of interest redduces.
- Rapid convergence of the ADM imposed for the said problem shows excellent result in simulating nano-bioconvection fluid dynamics problems.

The Newtonian nanofluids considered in the present problem are taken care of with *disk stretching*. Future investigations can be obtained by considering various models of *non-Newtonian nanofluids*. These investigations will also utilize ADM and other numerical techniques (finite element method). Furthermore, wavy geometries for the disk surfaces may be considered [42,43] as well as thermophysical properties [44] which also constitutes interesting extensions to the present work. Porous media [45], onset of bioconvection [46] and specifically water based nanofluid bio convection [47] may also be examined.

Nomenclature

$\tilde{b}$ Chemotaxis constant
$\bar{C}$ nanoparticle volume fraction
$\bar{C}_f$ fluid concentration
$Cf_{\bar{r}}$ axial skin friction coefficient
$Cf_{\bar{\theta}}$ tangential skin friction coefficient
C_w wall concentration
C_∞ free stream concentration
D_B Brownian diffusion coefficient (m^2/s)
D_n Microorganism diffusion coefficient (m^2/s)
D_T thermophoretic diffusion coefficient (m^2/s)
$f(\eta)$ axial stream function
f_w Stefan blowing parameter
$g(\eta)$ circumfrential stream function
h_m convective fluid concentration
Le ordinary Lewis number
Lb bioconvection Lewis number
m_w surface mass flux (W/m^2)
Nb Brownian motion parameter
Nd Biot number
Nt thermophoresis parameter
$Nu_{\bar{r}}$ local Nusselt number
$\bar{n}$ number of motile microrganism
$\bar{N}_w$ motile microorganism at the wall
P constant fluid pressure
Pe bio convection Peclet number
Pr Prandtl number
q_n surface microorganism flux
q_w wall heat flux (W/m^2)
$Qn\bar{r}$ local wall motile microoganism
$\bar{r}$ axial coordinate (m)
$\mathrm{Re}\bar{r}$ local Reynolds number
S unsteadiness parameter
$Sh\bar{r}$ local Sherwood number
t time (s)
$\bar{T}$ nanofluid temperature (K)
$\bar{T}_f$ fluid temperature (K)
T_w wall temperature (K)
T_∞ free stream temperature (K)
$\bar{u}_{\bar{r}}$ velocity component along the $\bar{r}$ axis(m/s)
$\bar{u}_{\bar{z}}$ velocity component along the $\bar{z}$ axis(m/s)
$\bar{u}_{\theta}$ velocity component along the $\bar{\theta}$ axis(m/s)
W_c maximum cell swimming speed (m/s)
$\bar{z}$ coordinate normal to the plate (m)

Greek letters

α thermal diffusivity (m^2 /s)
α_c strength of disk radial stretching
β constant
$\psi(\eta)$ number of motile microrganism
$\phi(\eta)$ nano particle volume fraction
η independent similarity variable
μ dynamic viscosity (Kg/ ms)
$\theta(\eta)$ temperature
ρ_f nanofluid density (Kg/m^3)
τ ratio of heat capacity of nanofluid and heat capacity of the fluid
$\tau_{\bar{r}}$ skin friction in $\bar{r}$ direction (Pa)
τ_θ skin friction in $\bar{\theta}$ direction (Pa)
ν Kinematic viscosity (m^2/s)
ψ stream function (m^2/s)
Ω angular velocity

References

[1] MA HT, ZHANG YF, DENG N, Mass transfer characteristics from a rotating cylinder, HEFAT 2008 6th International Conference on Heat Transfer, Fluid Mechanics and Thermodynamics, 2008, 30 June to 2 July, Pretoria, South Africa.

[2] MOHANTY AK, TAWFEK AA, PRASAD BVSS, Heat transfer from a rotating cylinder in crossflow, Experimental Thermal and Fluid Science, 1995, 10:54-61.

[3] ANWAR BEG O, PRASAD VR, VASU B, GORLA RSR, Computational modelling of magnetohydrodynamic convection from a rotating cone in orthotropic Darcian porous media, Journal of Brazilian Society of Mechanical Science Engineering, 2017, 39:2035-2054.

[4] SUBHASHINI SV, TAKHAR HS,NATH G, Non-uniform mass transfer or wall enthalpy into a compressible flow over a rotating sphere, Heat and Mass Transfer, 2007, 43(11):1133–1141.

[5] TAKHAR HS, WHITELAW MH, Higher order heat transfer from a rotating sphere, Acta Mechanica, 1978, 30:101–109.

[6] FRANCESCHINI EA, LACCONI GI, CORTI HR, Kinetics of hydrogen evolution reaction on nickel modified by spontaneous Ru deposition: A rotating disk electrode and impedance spectroscopy approach, International Journal of Hydrogen Energy, 2016, 41(5):3326-3338.

[7] TANG T, LI K, YING D, SUN T, WANG Y, JAI J, High efficient aqueous-film rotating disk photocatalytic fuel cell (RDPFC) with triple functions: Cogeneration of hydrogen and electricity with dye degradation, International Journal of Hydrogen Energy, 2014, 39(19):10258-10266.

[8] PEEV G, PESHAV D, NIKOLOVA A, Gas absorption in a thin liquid film flow on a horizontal rotating disk, Heat and Mass Transfer, 2007, 43(8):843–848.

[9] KARMAN TV, Uber laminare und turbulent Reibung. ZAMM, 1921, 1:233–252.

[10] GREENSPAN H, The Theory of Rotating Fluids, Cambridge University Press, New York, 1968.

[11] SHEVCHUK IV, Convective Heat and Mass Transfer in Rotating Disk Systems, Springer, New York, 2009.

[12] GAMBARYAN-ROISMAN T, STEPHAN P, Hydrodynamics and heat transfer in a liquid film flowing over a spinning disk with specific wall topography, ASME 2011 9th International Conference on Nanochannels, Microchannels, and Minichannels. 2011, June 19–22, Edmonton, Alberta, Canada.

[13] HELCIG C, WIESCHE SAD, Effect of Prandtl number on the heat transfer from a rotating disk: an experimental study, ASME 2016 Heat Transfer Summer Conference 2016, July 10–14, Washington DC, USA.
[14] CHOI SUS, Enhancing thermal conductivity of fluids with nanoparticles, developments and applications of non-Newtonian Flows, American Society of Mechanical Engineers, New York, 1995, 99–105.
[15] BUONGIORNO J, Convective transport in nanofluids, ASME Journal of Heat Transfer, 2006, 128(3):240–250.
[16] DAS SK, CHOI SUS, YU W, PRADEEP T, Nanofluids: Science and Technology, John Wiley, New York, 2007.
[17] TURKYILMAZOGLU M, Nanofluid flow and heat transfer due to a rotating disk, Computers & Fluids, 2014, 94:139-146.
[18] HAYAT T, IMTIAZ M, ALSAEDI A, ALZAHRANI F, Effects of homogeneous–heterogeneous reactions in flow of magnetite-Fe_3O_4 nanoparticles by a rotating disk, Journal of Molecular Liquids, 2016, 216:845-855.
[19] RAZA J, ROHINI AM, OMAR Z, AWAIS M, Heat and mass transfer analysis of MHD nanofluid flow in a rotating channel with slip effects, Journal of Molecular Liquids, 2016, 219:703-708.
[20] CHAKRABORTY T, DAS K, KUNDU PK, Framing the impact of external magnetic field on bioconvection of a nanofluid flow containing gyrotactic microorganism with convective boundary conditions, Alexandria Engineering Journal, 2016, 57(1): 61-71.
[21] XUN S, ZHAO J, ZHENG L, ZHENG X, Bio convection in rotating system immersed in nanofluid with temperature dependent viscosity and thermal conductivity, International Journal of Heat and Mass Transfer, 2017, 111:1001-1006.
[22] ANWAR BEG O, BASIR MFM, UDDIN MJ, ISMAIL AIM, Numerical study of slip effects on asymmetric bio convective nanofluid flow in a porous microchannel with an expanding/contracting upper wall using Buongiorno's model, Journal of Mechanics in Medicine and Biology, 2017, 17 (5):1750059-1.
[23] LI JJ, LU H, RAEES A, ZHAO QK, Unsteady mixed bio convection flow of a nanofluid between two contracting or expanding rotating discs, Zeitschrift für Naturforschung A, 2017, 71(3):1-12.
[24] IMTIAZ M, HAYAT T, ALSAEDI A, AHMAD B, Convective flow of carbon nanotubes between rotating stretchable disks with thermal radiation effects, International Journal of Heat and Mass Transfer, 2016, 101:948-957.
[25] HAYAT T, QAYYUM S, IMTIAZ M, ALZAHRANI F, ALSAEDI A, Partial slip effect in flow of magnetite-Fe_3O_4 nanoparticles between rotating stretchable disks, Journal of Magnetism and Magnetic Materials, 2016, 413:39-48.
[26] HAYAT T, QAYYUM S, IMTIAZ M, F. ALZAHRANI F, ALSAEDI A, Radiative flow due to stretchable rotating disk with variable thickness, Results in Physics, 2017, 7:156-165.
[27] AHMED N, ADNAN, MOHYUD-DIN UST, Influence of shape factor on flow of magneto-nanofluid squeezed between parallel disk, Alexandria Engineering Journal, 2017. https://doi.org/10.1016/j.aej.2017.03.031.
[28] MUSHTAQ A, MUSTAFA M, Computations for nanofluid flow near a stretchable rotating disk with axial magnetic field and convective conditions, Results in Physics, 2017, 7:3137-3144.
[29] CHEN H, CHEN J, GENG Y, CHEN K, Three-dimensional boundary layer flow over a rotating disk with power-law stretching in a nanofluid containing gyrotactic microorganisms, Heat Transfer-Asian Research, 2017. https://doi.org/10.1002/htj.21327.
[30] LATIFF NA, UDDIN MJ, ISMAIL AIM, Stefan blowing effect on bio convective flow of nanofluid over a solid rotating stretchable disk, Propulsion and Power Research, 2016, 5(4): 267-278.
[31] WATSON LT, WANG CY, Deceleration of a rotating disk in a viscous fluid, Physics of Fluids, 1979, 22:2267-2275.
[32] SHAMSHUDDIN MD, ANWAR BEG O, SUNDER RAM M, KADIR A, Finite element computation of multi-physical micropolar transport phenomena from an inclined moving plate in porous media, Indian Journal of Physics, 2017, 92(2): 215-230.
[33] ZOHRA FT, UDDIN MJ, ISMAIL AIM, ANWAR BEG O, KADIR A, Anisotropic slip magneto-bio convection flow from a rotating cone to a nanofluid with Stefan blowing effects, Chinese J. Phys. 2017, 56(1):432-448.
[34] DANIEL YS, DANIEL SK, Effects of buoyancy and thermal radiation on MHD flow over a stretching porous sheet using homotopy analysis method, Alexandria Engineering Journal, 2015, 54(3):705-712.
[35] BHATTI MM, SHAHID A, ANWAR BEG O, KADIR A, Numerical study of radiative Maxwell viscoelastic magnetized flow from a stretching permeable sheet with the Cattaneo–Christov heat flux model, Neural Computing & Applic. 2017,30(11):3467-3478. https://doi.org/10.1007/s00521-017-2933-8.
[36] ADOMAIN G, Solving Frontier Problems in Physics: The Decomposition Method, Kluwer, Dordrecht, USA, 1994.
[37] HAQ F, SHAH, K, GHAUS UR RAHMAN, SHAHZAD M, Numerical solution of fractional order smoking model via Laplace Adomian decomposition method, Alexandria Eng. J. 2017, 57(2):1061-1069. https://doi.org/10.1016/j.aej.2017.02.015.
[38] ANWAR BEG O, TRIPATHI D, SOCHI T, GUPTA PK, Adomian decomposition method (ADM) simulation of magneto-bio-tribological squeeze film with magnetic induction effects, Journal of Mechanics Medicine Biology, 2015, 15:1550072.1-1550072.23.
[39] AHLERSTEN K, An introduction to MATLAB, Bookboon publishers, 2015.
[40] EVANS DJ, The rotationally symmetric flow of a viscous fluid in the presence of an infinite rotating disc with uniform suction, Quarterly Journal of Mechanics and Applied Mathematics, 1969, 22(4):467-485.
[41] FANG T, TAO H, unsteady viscous flow over a rotating stretchable disk with deceleration, Communication in Nonlinear Science and Numerical Simulations, 2012, 17(12):5064-5072.
[42] SIDDIQA S, GUL-E-HINA, BEGUM N, SALEEM S, HOSSAIN MA, GORLA RSR, Numerical solutions of nanofluid bioconvection due to gyrotactic microorganisms along a vertical wavy cone, International Journal of Heat and Mass transfer, 2016, 101:608-613.
[43] SIDDIQA S, SULAIMAN M, HOSSAIN MA, ISLAM S, GORLA RSR, Gyrotactic bioconvection flow of a nanofluid past a vertical wavy surface, International Journal of Thermal Sciences, 2016, 108:244-250.
[44] BEGUM N, SIDDIQA S, HOSSAIN MA, Nanofluid bioconvection with variable thermophysical properties, Journal of Molecular Liquids, 2017, 231:325-332.
[45] SAINI S, SHARMA YD, Analysis of onset of bio-thermal convection in a fluid containing gravitactic microorganism by the energy method, Chinese Journal of Physics, 2018, 56(5): 2031-2038.
[46] SAINI S, SHARMA YD, Analysis of onset of bio-thermal convection in a fluid containing gravitactic microorganism by the energy method, Chinese Journal of Physics, 2018, 56(5): 2031-2038.

[47] SAINI S, SHARMA YD, A Bio-Thermal convection in waterbased nanofluid containing gyrotactic microorganism: Effect of vertical throughflow, Journal of Applied Fluid Mechanics, 2018, 11(4):895-903.

Received date: 0000−00−00; **Accepted date:** 0000−00−00
Corresponding author: Shamshuddin MD

(Edited by HE Yun-bin)

Foundation item: P